Seismic cycles, size of the largest events, and the avalanche size distribution in a model of seismicity

L. E. Aragón[*] and E. A. Jagla

Centro Atómico Bariloche and Instituto Balseiro, Comisión Nacional de Energía Atómica, 8400 Bariloche, Argentina

A. Rosso

Laboratoire de Physique Théorique et Modèles Statistiques, CNRS, Université Paris-Sud, 91405 Orsay, France

We address several questions on the behavior of a numerical model recently introduced to study seismic phenomena, which includes relaxation in the plates as a key ingredient. First, we make an analysis of the scaling of the largest events with system size and show that, when parameters are appropriately interpreted, the typical size of the largest events scale as the system size, without the necessity to tune any parameter. Second, we show that the temporal activity in the model is inherently nonstationary and obtain from here justification and support for the concept of a "seismic cycle" in the temporal evolution of seismic activity. Finally, we ask for the reasons that make the model display a realistic value of the decaying exponent b in the Gutenberg-Richter law for the avalanche size distribution. We explain why relaxation induces a systematic increase in b from its value $b \simeq 0.4$ observed in the absence of relaxation. However, we have not been able to justify the actual robustness of the model in displaying a consistent b value around the experimentally observed value $b \simeq 1$.

PACS number(s): 89.75.Da, 91.30.Ab, 05.65.+b, 46.65.+g

I. INTRODUCTION

Modeling of seismic phenomena as a statistical mechanic process has a long history that goes back almost to the very beginning of plate tectonics. There are a lot of variables affecting seismic activity, and many of them cannot be taken into account in a simplified theoretical description. However, if a model gives a sequence of events strongly resembling real ones (in its temporal, spatial, and magnitude distribution), it is tempting to consider that the model captures those key ingredients playing an important role in the production of seismic events. This is what happens with the model proposed by Burridge and Knopoff [1,2]. Constructed in the form of a large collection of repetitive and simple elements (rigid blocks interacting through elastic springs and sliding on a rigid surface), it displays nontrivial features, most remarkably the existence of avalanches (earthquakes) with a broad distribution of sizes. Based on the work of Burridge and Knopoff, in 1991 Olami, Feder, and Christensen (OFC) [3] introduced a model that has become one of the paradigms of simulation of seismic activity. The model is presented in the form of cellular automata, and the dynamics is defined as a list of rules. A broad distribution of event sizes is obtained with the OFC model. Despite the attention it received, the OFC model displays a series of unrealistic features when trying to model seismic phenomena. For instance, the prominent spatial and temporal correlation of events that is observed in the field, mostly the existence of aftershocks, is not reproduced [4]. Also, obtaining a realistic value of the b exponent in the Gutenberg-Richter (GR) law requires the tuning of an internal parameter of the model.

In the last years, we have been working on introducing modifications to this kind of model in such a way that more realistic sequences of events are obtained. The two crucial modifications we have proposed are [5,6] (see a more detailed account in the next section) the consideration of variable thresholds (instead of the constant value considered by OFC) and the incorporation of a mechanism of internal (also called structural) relaxation, quantified by a parameter R. With these two ingredients we have obtained a model in which (i) the spatial and temporal correlation of events is comparable to that of real ones, in particular, aftershock sequences obeying the Omori law [7] are obtained; (ii) the avalanche size distribution has a GR form, with an exponent b very close to actually observed values (around 1); and (iii) the friction properties derived from the model reproduce nontrivial results such as velocity weakening and the stress peak in experiments of slip-stop-slip [8]. It is worth mentioning that as long as R is larger than some threshold value, all these results are obtained irrespective of the precise value of R.

The number of realistic features that have been obtained with this model encouraged us to go further and investigate in more depth its properties to better understand how they originate in the existence of the relaxation process. This is the aim of the present work. To make the presentation self-contained, in the next section the model is explained with all necessary detail, in the case without relaxation, $R = 0$, and in the presence of relaxation, $R \neq 0$. Also, a limiting case of infinite relaxation $R \to \infty$ is introduced, which is interesting to consider throughout the paper.

In Sec. III we review some results obtained in the case $R = 0$. It is shown that this case is equivalent to the problem of depinning of an elastic interface in a random medium. We also give a comparison of the results obtained at "constant driving velocity" with those at "constant force," showing that there is a clear mapping between the two.

In Sec. IV we show that when $R \neq 0$ we cannot make an equivalence between simulations at constant velocity and constant force. In fact, in constant velocity simulations at $R \neq 0$, there are systematic fluctuations of the stress on the system that make the problem nonstationary, and this generates a scenario in which a description in terms of a "seismic cycle" naturally emerges.

———————
[*]aragonl@ib.cnea.gov.ar

In Sec. V we discuss the scaling of the linear size of the largest events $L_{\max}$ with the control parameter α. We show that with an appropriate interpretation of α as inversely proportional to the thickness of the sliding slabs, there are events that are comparable in size with the size of the system. This is a consequence of the existence of relaxation and does not occur in the $R = 0$ case.

Section VI is devoted to the following issue: the model with $R = 0$ gives a consistent (although unrealistic) value for the b exponent of about $b \simeq 0.4$. The inclusion of relaxation drives this exponent to values closer to the realistic value $b \simeq 1$, without tuning of any parameters. What is the reason for this behavior? As we see, we are only in the position to provide a partial answer to this question.

Finally, in Sec. VII, we make a brief summary and present our conclusions.

II. MODELS

A. OFC model

Our starting point is the cellular automata model proposed by OFC [3] to describe seismicity. The OFC model considers a set of real-valued variables u_i, where i indicates the position in a two-dimensional lattice. u_i is interpreted as the force that a rigid substrate exerts on a solid block at position i, and it represents the local stress between the sliding plates (see Fig. 1). The system is driven by uniformly increasing the values of u_i with time at a rate V, simulating the tectonic loading of the plates. Every time one of the variables u_i reaches
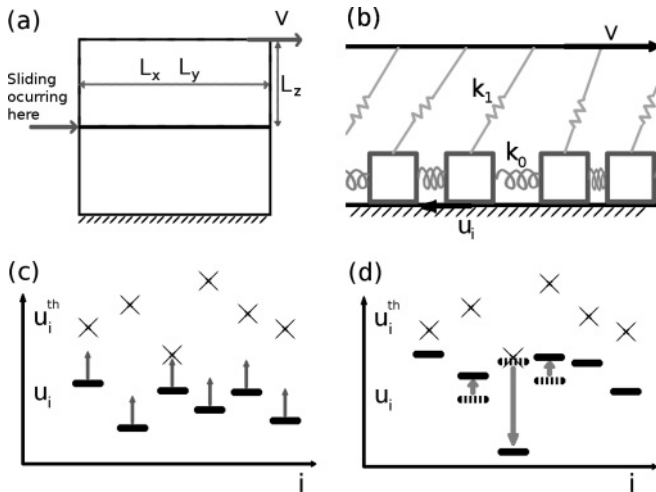

FIG. 1. Sketch of the sliding situation that we study. (a) Two solid blocks slide against each other due to a constant driving between the top and the bottom planes. Their relative velocity is V. Dimensions of the blocks are L_x, L_y in the sliding plane and L_z perpendicular to it. (b) The solids in (a) are replaced by a rigid surface and an array of small blocks joined by springs of stiffness k_0. Driving acts on each block through a spring of stiffness k_1. Note that the value of k_1 is inversely proportional to L_z in (a). (c) Values of friction forces u_i and maximum forces u_i^{th} at each site are shown for the OFC* model. Friction forces increase uniformly (as indicated by the arrows) as driving proceeds. (d) The prescription as one u_i reaches the local threshold: u_i decreases by 1 unit, and the neighbors increase their u values by a quantity α.

a maximum value (ordinarily set to a uniform, dimensionless value of 1), the local stress u_i is "discharged" by setting it to 0. This local stress drop Δu produces a stress increase onto neighbor blocks according to $u_j \rightarrow u_j + \alpha \Delta u$, where j indicates a neighbor site to i. The value of α can vary between 0 and $\alpha_c \equiv 1/Z$, Z being the number of neighbors in the lattice. We refer only to the case of a square lattice, so $Z = 4$, $\alpha_c = 1/4$. The case $\alpha = \alpha_c$ is called the conservative case, whereas $\alpha < \alpha_c$ are nonconservative cases. In the mechanical interpretation of the model, the value of α is related to the stiffness of the springs that interconnect the blocks and springs that push from the blocks at velocity V [see Fig. 1(b)]. The actual relation is $\alpha = k_0/(k_1 + 4k_0)$. A discharge event can produce the overpass of the maximum local stress on one or more than one neighbor, and in this way a large cascade can be generated. This cascade is called an event and is identified with an individual earthquake (note that the complete cascade is assumed to occur at a constant time, namely, earthquakes are instantaneous). The size S of an event is defined as the sum of all discharges that compose the event, and the magnitude is defined as $M = \frac{2}{3} \log_{10} S$, so as to match (up to an additive constant) the usual definition used in geophysics [9].

The OFC model is typically simulated using open boundary conditions; otherwise, the spatial homogeneity generated by the use of periodic conditions induces a strong global synchronization in the model. The OFC model displays an exponential decay of number of events as a function of magnitude (or a power-law decay if expressed in terms of S) compatible with a GR law of the form $N(M) \sim 10^{-bN}$. The b value depends on the value of α. Realistic values of b are obtained for $\alpha \simeq 0.2$.

B. OFC* model

The maximum values that the variables u_i can withstand in the OFC model are set to a constant, uniform value of 1. Having in mind the realistic situation of a heterogeneous fault, with the constitutive materials having different properties at different positions, it becomes natural to consider a case in which the threshold values are not constant but have some spatial variation. This is the first modification we introduce into the OFC model. Concretely, the values of the local thresholds are called u_i^{th}, and we draw them from some random distribution. Each time u_i overpasses the local threshold u_i^{th}, u_i is updated to a new value. We use the update rule $u_i \rightarrow u_i - 1$; i.e, we implement the prescription of a unitary local stress drop. Upon this drop in the local stress, the values of u on neighbor sites are updated as before, namely, $u_j \rightarrow u_j + \alpha$, for j neighbor to i [see Figs. 1(c) and 1(d)]. Every time u_i is updated, a new value is assigned to the local threshold u_i^{th}, taken from its original random distribution. This prescription is justified by the same physical arguments as before, since the sliding pieces can reasonably be thought of as finding different maximum strengths as sliding proceeds. We refer to the OFC model with this modification as the OFC* model.

The results obtained with the OFC* model differ qualitatively from those obtained with the OFC model. In particular, the b exponent becomes α independent, taking a value of around $b \simeq 0.4$ (still quite unrealistic for earthquakes). Interestingly, now the maximum avalanche size is controlled

by the value of α, diverging for $\alpha \to \alpha_c$ (assuming an infinite spatial extent of the system). This may be considered a weak point, since it seems to indicate that it is not sufficient to have an infinitely large system to have critical behavior; the condition $\alpha \to \alpha_c$ is also needed. However, we see in Sec. V that this argument is flawed, as the large system size limit also implies $L_z \to \infty$, and in this limit we naturally obtain that $\alpha \to \alpha_c$.

C. OFCR model

The second and crucial modification we made to the OFC model is the introduction of internal relaxation effects. We do not repeat here the arguments that justify its introduction, but let us just mention the following fact that points to the necessity of these effects: In the OFC, or OFC* models, a sudden stop of tectonic loading causes all seismic activity to cease at once. This is unrealistic, as, for instance, the processes that trigger aftershocks after a main event depend on the rearrangements that occur in the fault after the main shock and are not directly related to tectonic loading. In other words, dynamical effects within the faults should be taken into account in order to have a realistic description of the seismic process. This is what we did by introducing the internal relaxation mechanism into the OFC* model. As this relaxation is controlled by a parameter R, we call this the OFCR model. The concrete implementation prescribes that the evolution of the variables u_i is given by

$$\frac{du_i}{dt} = R(\nabla^2 u)_i + V; \tag{1}$$

namely, in addition to the external loading (represented by the V term), there is a tendency to make the values of u_i progressively more uniform in the system. This relaxation term produces the appearance of aftershocks and realistic friction properties in the system. In addition, the exponent of the GR law is modified, acquiring a value consistent with observations. [5,6]

For the rest of the paper it is important to consider a couple of variations of the previous relaxation mechanism. One of them is to consider relaxation in a "mean-field" manner. By this we understand that, instead of the sum over the neighbor sites implied by the Laplacian operator in Eq. (1), we take the average over the whole system, i.e, noting $\bar{u}$, the mean value of u_i, we have

$$\frac{du_i}{dt} = -4R(u_i - \bar{u}) + V \tag{2}$$

(the factor of 4 is included to make a more direct comparison between the R parameters in the two equations). Consideration of relaxation in the mean field is important because it allows very efficient determination of the next site that becomes unstable (i.e., the first site for which u_i reaches u_i^{th}), as Eq. (2) can be solved analytically, whereas the same determination for Eq. (1) requires a time-consuming integration scheme. Results using both schemes of relaxation do not differ substantially. A comparison between the two schemes was presented in Ref. [5].

The second special case considered is the limit of "infinite relaxation" defined by the condition $R/V \to \infty$. In this limit, there is a clear-cut separation between events that are triggered by the tectonic loading V term in Eq. (1) or (2) and those that are triggered by the relaxation term proportional to R. In fact,

in this case events separate naturally into "clusters." In between successive clusters, the spatial distribution of u_i is uniform, and the V term acts, moving up all u_i uniformly until the lowest u^{th} is reached. At this point, an event is triggered that leaves the u's in a nonuniform state, over which the relaxation term acts. Under this action, aftershocks are triggered until the spatial distribution of u's becomes uniform again, and the process is repeated.

III. BACKGROUND MATERIAL ON THE $R = 0$ CASE

We present in this section a few reference results for the case of no relaxation, but with variable thresholds, namely, what we have called the OFC* model.

A. Mapping between elastic interfaces in random media and the OFC* model

Different authors have explored the relation between the deppining transition of an elastic interface and spring-block, sandpile, or charge-density wave models [10–12]. Here we show that the OFC* model can be mapped onto the problem of a two-dimensional elastic interface close to the depinning transition.

Let us consider an ensemble of block positions h_i identifying a two-dimensional interface. The energy of a given interface can be written as the sum of three contributions.

(1) The elastic energy between nearest-neighbors blocks: $E_1 = \frac{k_0}{2} \sum_{\langle i,j \rangle} (h_i - h_j)^2$, where h_i and h_j are the positions of blocks i and j, and k_0 is the "surface tension" of the elastic interface.

(2) The energy of tectonic loading: $E_2 = \sum_i \frac{k_1}{2}(h_i - Vt)^2$, where V measures the rate and k_1 is the stiffness of the loading.

(3) The random energy associated with the block position h_i, which is responsible for the pinning of the blocks.
Elastic interactions and tectonic loading generate a force $F_i = -\partial_{h_i}(E_1 + E_2)$ which competes with the pinning force $F_{\text{pinn}}(h_i)$ induced by the random energy. The force F_i acting on each block increases with time because of the loading. When F_i overcomes $F_{\text{pinn}}(h_i)$, the block i becomes unstable and its position is increased by 1 ($h_i \to h_i + 1$). As a consequence, (i) the force F_i drops to $F_i - (4k_0 + k_1)$, (ii) a new pinning force is associated with the new position $h_i + 1$, and (iii) the force acting on the neighboring blocks increases, $F_j \to F_j + k_0$.

The dynamics of this interface in the presence of a disordered landscape can be easily identified with OFC* dynamics in the presence of variable thresholds, the stress u_i being $F_i/(k_1 + 4k_0)$ and the control parameter α being $k_0/(k_1 + 4k_0)$.

B. Review of the depinning transition

The zero-temperature motion of an elastic interface in random media has been studied in detail in the last two decades [13–16]. Two dynamical protocols are possible: (i) *constant velocity*, which corresponds to the OFC* model with a tectonic loading; and (ii) *constant force*, where the parabolic tectonic loading E_2 is replaced by the action of a constant and uniform stress σ, and the force acting on block i writes $F_i = (-\partial_{h_i} E_1) + 4k_0\sigma$.

1. Constant force

For a given (and low) σ the interface is pinned in a metastable state for which the forces acting on all the blocks are smaller than the forces induced by the pinning centers. When σ is increased by an infinitesimal amount $\delta\sigma$, two things can happen: (i) either the metastable state remains metastable or (ii) the metastable state becomes unstable and moves to a new metastable position. The distance between the old pinned position and the new one can be measured as the volume S included between the two consecutive metastable states. This volume represents the size S of the event. A critical threshold σ_c exists, above which there are no metastable states, and the interface evolves indefinitely. The transition between the pinned phase, $\sigma < \sigma_c$, and the moving phase, $\sigma > \sigma_c$, is called depinning.

Results of simulations at different values of $\sigma < \sigma_c$ show that the distribution of events follows a power law, with a large size cutoff, $S_{\max}(\sigma)$, and an exponent $\tau > 1$:

$$N(S) \propto \frac{1}{S^\tau} f\left(\frac{S}{S_{\max}(\sigma)}\right). \quad (3)$$

The exponent τ used by the statistical mechanics community is related to the exponent b typically used by geophysicists when looking at real earthquakes. The relation between them is given by $\tau = 1 + 2b/3$. We refer mainly to values of τ from now on. The function $f(S/S_{\max})$ has a fast decay when $S \gg S_{\max}$ and the characteristic large size $S_{\max}(\sigma)$ diverges as σ reaches a critical threshold σ_c. The divergence of $S_{\max}$ goes with the divergence of the linear size of the maximal avalanche $L_{\max}$. $L_{\max}$ is often seen as the "growing correlation length" associated with this dynamical phase transition, and close to σ_c, $L_{\max}$ behaves as $(\sigma_c - \sigma)^{-\nu}$, where the positive exponent ν is defined in analogy with the correlation length exponent of equilibrium critical phenomena.

Large avalanches occur because the system is "organized" at large distances; another consequence of this "organization" is that the interface is a correlated object displaying a power-law roughness. A positive roughness exponent ζ can be defined from the growth of the distance between blocks $|h_i - h_j| \sim |i - j|^\zeta$. An argument based on a symmetry of the system (statistical tilt symmetry) [14–16] allows us to relate the exponent ν to the exponent ζ, yielding

$$\nu = \frac{1}{2 - \zeta}. \quad (4)$$

From basic dimensional arguments we can write

$$S_{\max} \sim L_{\max}^{2+\zeta} \sim (\sigma_c - \sigma)^{-\nu(2+\zeta)} \sim (\sigma_c - \sigma)^{-\frac{2+\zeta}{2-\zeta}}. \quad (5)$$

An important scaling relation between τ and ζ can be established if we compute the average size of an event $\bar{S}$. On one hand, using the scaling form of Eq. (3), this quantity can be written in terms of the cutoff size, in the form $\bar{S} \propto S_{\max}^{2-\tau}$, as long as $1 < \tau < 2$, which is always the case here. On the other hand, we observe that the displacement of the center of mass $x_{\mathrm{c.m.}}$ of the interface when the stress in increased by an infinitesimal amount can be written as $x_{\mathrm{c.m.}}(\sigma + \delta\sigma) - x_{\mathrm{c.m.}}(\sigma) = \bar{S} N_\sigma(\delta\sigma)/(L_x L_y)$, where $N_\sigma(\delta\sigma)$ is the number of events when the stress jumps from σ to $\sigma + \delta\sigma$. If this number does not diverge when the threshold

is approached (as confirmed by all simulations), then we can power expand, and to leading order we have $N_\sigma(\delta\sigma) \sim c_1 \delta\sigma L_x L_y + \cdots$. Thus, it follows that the average size of an event is proportional to $\bar{S} \sim \delta x_{\mathrm{c.m.}}/\delta\sigma \equiv \chi$, the susceptibility of the interface. As the critical threshold is approached the interface moves more and more, the position of the interface grows as $x_{\mathrm{c.m.}}(\sigma) \sim L_{\max}^\zeta$, and thus the susceptibility diverges as $\chi \sim (\sigma_c - \sigma)^{-\nu\zeta - 1}$. We thus obtain

$$\nu(2 + \zeta)(2 - \tau) = \nu\zeta + 1 \quad \Longrightarrow \quad \tau = 2 - \frac{\zeta + \frac{1}{\nu}}{2 + \zeta}. \quad (6)$$

Using the statistical tilt symmetry relation Eq. (4), we obtain

$$\tau = 2 - \frac{2}{2 + \zeta}. \quad (7)$$

2. Constant velocity

At a constant velocity, instead of a uniform stress, we have the parabolic potential E_2 centered at Vt. The interface embedded in this potential can be rough only at short length scales. The crossover between the short-distance regime, characterized by a rough interface, and the long-distance regime, with a flat interface, can be determined by dimensional analysis of the term $E_1 \sim L^{2\zeta}$ versus the term $E_2 \sim k_1 L^{2\zeta+2}$. The crossover length can be identified with the correlation length $L_{\max} \sim 1/\sqrt{k_1}$. Using the statistical tilt symmetry of elastic systems it is possible to show that this identification is actually correct. It is easy to verify that $\alpha_c - \alpha \sim k_1$, so that $\alpha_c - \alpha \simeq L_{\max}^{-2}$.

C. Results for the OFC* model

The previous arguments are consistent with the results of our simulations in the OFC* model. In Fig. 2 we show a sequence of individual events and the corresponding stress as a function of time for a fixed α and the event size distribution obtained for different values of α. A value $\tau \simeq 1.27$ is systematically observed. Also, from the distributions of $N(S)$
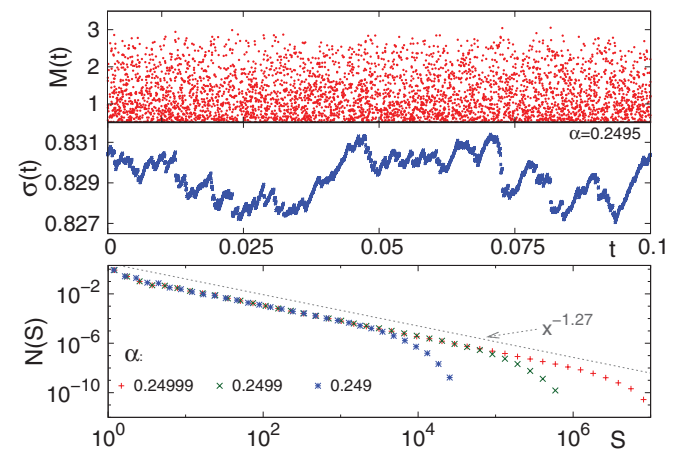

FIG. 2. (Color online) Magnitude-time and stress-time plot for the OFC* model, and the event size distribution obtained for three values of α as indicated. These distributions are very well fitted by a power law with an exponential cutoff.
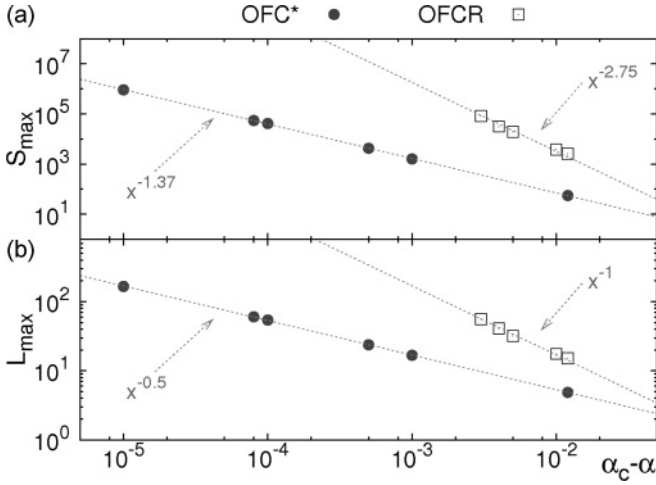
FIG. 3. Scaling of (a) S_{max} and (b) L_{max} with $(\alpha_c - \alpha)$ for the OFC* and the OFCR models, shown by filled and open symbols, respectively.

FIG. 4. Time-averaged values of σ as a function of the values of α for the OFC* model. Inset: The power-law dependence close to $\alpha_c = 0.25$, $\sigma_c \simeq 0.84236$ is emphasized in this logarithmic plot.

and the corresponding ones for $N(L)$ (L is the typical linear size of the avalanches), we obtain the value of the large-scale cutoff S_{max} and the maximum linear size L_{max} as a function of α for the OFC* model. Results are presented in Fig. 3. We found $S_{max} \sim (\alpha_c - \alpha)^{-\gamma}$ with $\gamma \simeq 1.37$, which is consistent with the ratio $\gamma = 1 + \zeta/2$ predicted by the theory of elastic interfaces of the previous section. We also find from Fig. 3 that $L_{max} \sim (\alpha_c - \alpha)^{-1/2}$, showing that statistical tilt symmetry is satisfied by the OFC* model, as the mapping to the elastic interface problem could have anticipated. As Narayan notes in the case of magnetic domain wall motion in Ref. [17], the cutoff diverges with system size; we discuss this topic in Sec. V.

For a fixed value of α we can follow the value of the average stress in the system (see Fig. 2), $\sigma \equiv \overline{u}_i$. The stress settles around a mean value, with fluctuations typical of finite-size effects. According to arguments in the previous section, the time-averaged σ vs α is expected to have a critical behavior as $\alpha \to \alpha_c$ of the form $(\sigma_c - \sigma) \simeq (\alpha_c - \alpha)^{1/(2\nu)}$ for some σ_c. This is verified in our numerical simulations (Fig. 4), as $1/(2\nu) \simeq 0.62$.

The existence of a well-defined average value of σ for each value of α allows us to recover the scaling relation Eq. (7) between τ and ζ using a slightly different argument. If an event of size S occurs in the system, it produces a reduction of σ by an amount proportional to $S\Delta\alpha/(L_x L_y)$ ($\Delta\alpha \equiv \alpha_c - \alpha$). If it is assumed (as it is in fact numerically verified) that the time interval between events does not become singular as $\Delta\alpha \to 0$, then there is a typical stress increment between events of the order of $1/(L_x L_y)$. To obtain a stationary mean value of σ, these two quantities have to compensate, on a temporal average; namely, we can write $\overline{S}\Delta\alpha \sim 1$, where, by $\overline{S}$, we note the average value of the events. Putting this estimation together with $\overline{S} \propto S_{max}^{2-\tau}$ and also using Eq. (5), we reobtain Eq. (7).

Simulations of the OFC* model at $\alpha < \alpha_c$ and a constant velocity are associated (in the mechanical analogy of the model) with driving by a finite-stiffness spring at a constant velocity. The univocal relation between α and σ also allows
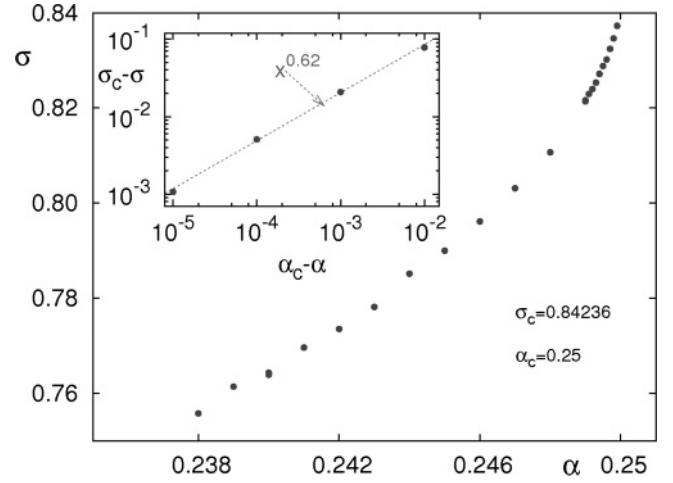
an alternative interpretation of the model, which is equivalent to driving the model at a constant force. Instead of applying a finite driving at fixed $\alpha < \alpha_c$, we set $\alpha = \alpha_c$, the driving velocity $V = 0$, and fix the mean value of σ from outside. A random site is chosen to initiate the avalanche. After the avalanche is exhausted, the process is repeated. Note that σ does not change in this process and remains equal to the externally imposed value. In this way of doing the simulation, after a transient period, the avalanche size distribution becomes stationary in time, and its statistics coincides with that obtained fixing a noncritical α and having a finite V, as shown in Fig. 5. The expected behavior of S_{max} as a function of σ is given in Eq. (5). This behavior is consistent with our data for which $\nu(2 + \zeta) \simeq 2.2$.

IV. OFCR MODEL AND THE SEISMIC CYCLE

In this section we begin to analyze results obtained in the presence of relaxation. We work in the limit of infinite
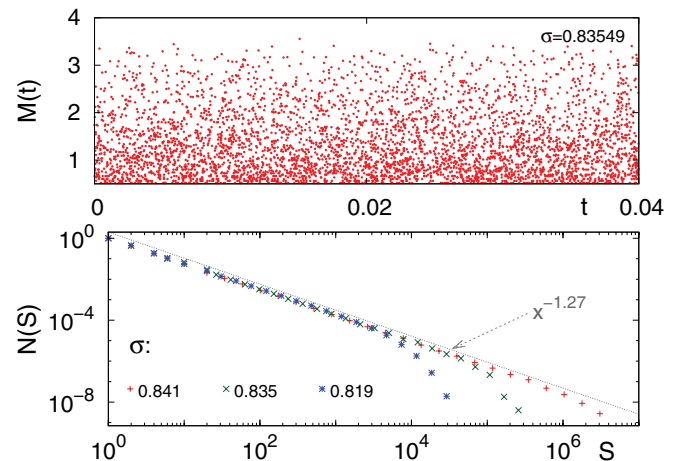

FIG. 5. (Color online) Magnitude-time plot for the OFC* model, taking $V = 0$ and $\alpha = 1/4$ and using the stress σ as a control parameter, and event size distribution obtained for three values of σ as indicated. Note the similarity to Fig. 2.
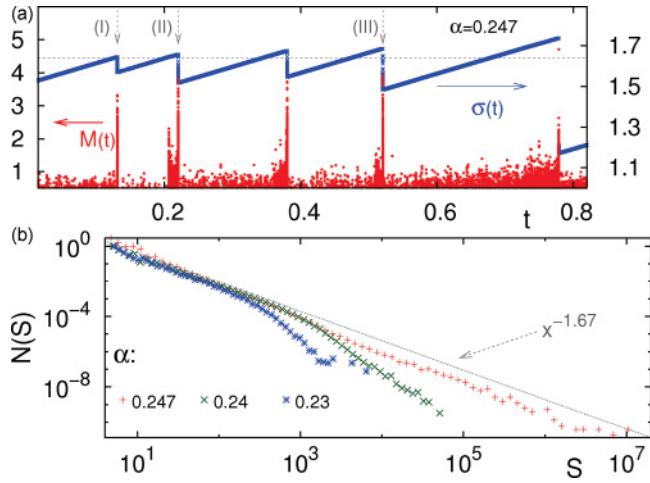
FIG. 6. (Color online) (a) Magnitude-time and stress-time plot for the OFCR model. The probability of large events is strongly enhanced every time some threshold value of the stress (roughly indicated by the dotted horizontal line) is passed. (b) The corresponding event size distribution for the whole sequence at different values of α.

relaxation and use the mean-field implementation of relaxation. A typical sequence of events for this case is shown in Fig. 6. We also indicate in that figure the evolution of σ over the simulation. In the infinite relaxation case we refer to an "internal" and an "external" temporal scale, which are totally decoupled. The external time scale is the scale of tectonic loading, and the internal time scale is the scale of relaxation in Eq. (1). In Fig. 6 we plot events as a function of the external time scale. This means that at a fixed value of the horizontal coordinate, we find a whole "cluster" of events. The events within some of these clusters, depicted as a function of the internal time scale, are shown in Fig. 7(a). One may consider that a cluster consists of a main shock and all the aftershocks it produces. The clear-cut identification of aftershocks as being linked to some main event can be unambiguously made only in the present case of full separation
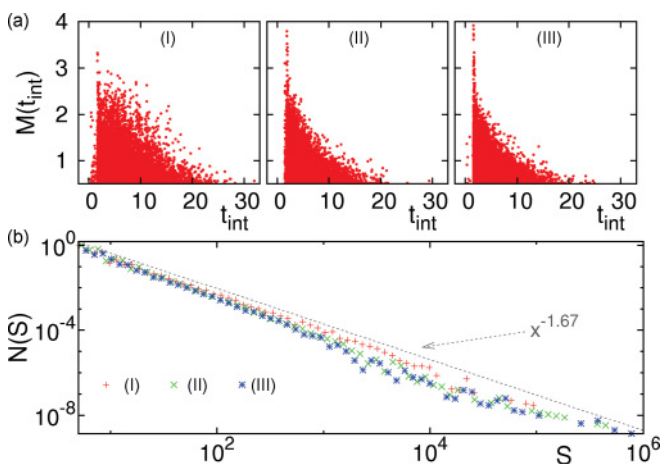

FIG. 7. (Color online) (a) Magnitude-internal time (t_{int}) for some of the main clusters observed in Fig. 6(a). t_{int} is measured in units of the relaxation parameter; i.e, a whole cluster here occurs at a single horizontal coordinate in Fig. 6(a). (b) The event size distribution of the individual clusters.

of time scales. Note, however, that within a cluster, the largest shock is not necessarily (or even usually) the first one. In any case, we can consider a cluster as the full sequence of events that is committed to appear once the first event has been triggered, in the case in which tectonic loading is stopped after the initial event. We emphasize that in the $R \rightarrow \infty$ case, not only is the value of σ shown in Fig. 6 the average value of u through the system, but also it is the actual value of every u_i.

From the results in Fig. 6 we see a systematic pattern of a steady increase in σ, followed by abrupt drops. We interpret this cycle of a smooth stress increase and sudden stress decrease as the manifestation in our model of a "seismic cycle" [9]. The concept of the seismic cycle suggests that stress on a fault builds up smoothly for a long period of time until it is suddenly released in a large earthquake, and the process starts over. This leads to the idea that large earthquakes in a given region occur in a quasiperiodic manner. This idea, however, has been difficult to verify: on one hand, because of the large time intervals between large earthquakes and, on the other hand, because deviations from periodicity could be so large as to transform a quasiperiodic sequence into something rather unpredictable. We note, however, that there have been a number of attempts (sometimes successful [18]) to infer the likelihood of the next large earthquake based on the record of previous large earthquakes in a particular region.

In the simulations, an alternation of large events and periods of rather low, slowly increasing activity is observed (see Fig. 6). However, this sequence is not periodic; instead, it looks like a more or less random process. In our case, we have the advantage of having access to all variables in the system, particularly to the instantaneous value of the stress, and thus we see that a large event occurs with a high probability once some typical value of the stress (roughly indicated by the dotted horizontal line in Fig. 6) has been passed. These observations point to the fact that there is some degree of predictability of the appearance of large earthquakes in the present model. However, we do not discuss this issue here, as we plan to elaborate in a forthcoming publication.

The fluctuations of stress during the seismic cycle for the OFCR model are more fundamental than those observed for the OFC* model in the previous section. Insight into this issue is provided by taking the data in Fig. 6 and plotting the total seismic moment S_c of each cluster (namely, the sum of the seismic moments of all events within a cluster) which is proportional to the stress drops observed in the curve of $\sigma(t)$ as a function of the value of stress at which the cluster is triggered. The result is shown in Fig. 8. We see that when σ is small, the clusters are typically small also and the stress drop caused by these relatively small clusters is not able to compensate the stress increase caused by tectonic loading. As σ becomes larger than a certain value (indicated by the dotted vertical line in Fig. 8), there is a finite probability that a very large cluster is triggered. The size of these large clusters diverges as $\alpha \rightarrow \alpha_c$. These large events generate the abrupt decrease in stress shown in Fig. 6, reinitiating the seismic cycle. This tells us that the fluctuations of stress in the OFCR model are a necessary part of the dynamics of the model, which is eminently nonstationary, and the existence of a seismic cycle is the manifestation of that.
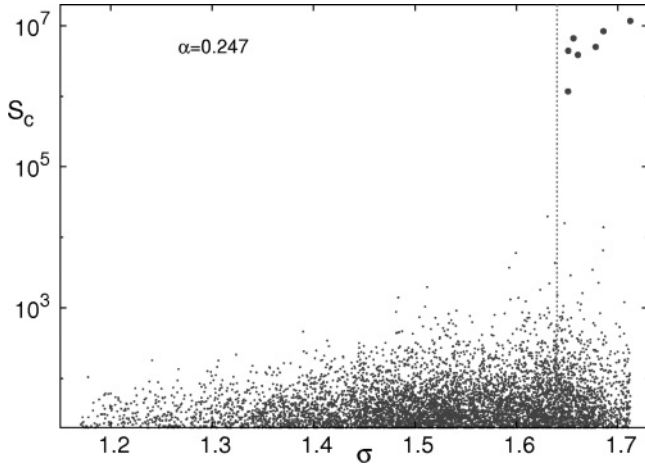
FIG. 8. The seismic moment of individual clusters S_c vs the initial value of stress at which they were triggered. Crossover stress (corresponding to the dotted horizontal line in Fig. 6) is indicated by the dotted vertical line. When stress becomes larger than this value there is some probability of triggering a very large cluster (these large clusters have been highlighted by using a larger symbol size).

V. MACROSCOPIC LIMIT OF THE OFCR MODEL

There is a clear-cut difference in the macroscopic limit of the OFC* and OFCR models, which shows that the OFCR model is a candidate to be a realistic model for describing seismicity, whereas the OFC* model is not. This is related to the scaling of the largest events observed for the two models in the macroscopic limit, which we discuss now.

This analysis starts from the key observation that the value of $\alpha_c - \alpha$ should be considered as being proportional to L_z^{-1}, where L_z indicates the thickness of the slabs that slide against each other. This is clear upon comparing Figs. 1(a) and 1(b): the value of k_1 [and thus of $\alpha_c - \alpha = k_1/4(4k_1 + k_0)$] is proportional to the restoring force the system exerts on a given displacement of the top plane of the slab. For a fixed displacement, the restoring force is inversely proportional to L_z, namely, $\alpha_c - \alpha \sim L_z^{-1}$.

In the macroscopic limit we should consider that L ($L \equiv L_x = L_y$; the two lengths in the x-y plane are taken equal for simplicity) and L_z go to macroscopic values, although not necessarily with the same tendency. We consider the case in which $L \gg L_z$; i.e., we maintain a sort of slab geometry. In this situation we want to calculate the maximum spatial extent $L_{\max}$ of the earthquakes in the x-y plane for the OFC* and OFCR models. In the first case the statistical tilt symmetry [verified in the numerical simulations; see Fig. 3(b)] implies that $L_{\max} \sim 1/(\alpha_c - \alpha)^{1/2}$, from which $L_{\max} \sim L_z^{1/2}$. This means that as L_z goes to infinity, the maximum spatial extent of the earthquakes becomes comparatively small. In other words, at large scales the sliding is smooth in the OFC* model, and earthquakes do not survive the macroscopic limit.

The situation is qualitatively different for the OFCR model. Here, numerical simulations indicate that the maximum spatial extent of the events has a different dependence on $(\alpha_c - \alpha)$. The results presented in Fig. 3(b) indicate a dependence $L_{\max} \sim 1/(\alpha_c - \alpha)$, which, in terms of L_z, can be written as

$L_{\max} \sim L_z$. This is a remarkable result. It indicates that no matter how large L_z is, the maximum size of earthquakes is a sizable fraction of it. We can thus say that, in this case, in the macroscopic limit earthquakes persist, and their maximum size scales as the system size itself. We think that this is a key point in the claim that this model can describe earthquakes in the macroscopic limit.

The finding of sizable earthquakes with size L_z can be correlated with other properties of the model. It is accepted in the geophysics community that systems in which earthquakes occur must have an effective friction law of the velocity weakening type [8,9]; namely, the average friction force must be a decreasing function of the velocity, at least in a velocity range relevant for the process. Actually, we have shown elsewhere [5] that the OFCR model does display velocity weakening, and in the origin of this behavior is again the existence of relaxation. It is immediate to show that such velocity weakening systems cannot sustain uniform sliding, and a stick-slip motion must necessarily occur for a sufficiently soft driving (i.e., for $\alpha \to \alpha_c$). Now if we assume a generic dependence of $L_{\max}$ on L_z of the form $L_{\max} \sim L_z^{\omega}$, the value $\omega < 1$ would correspond to an asymptotically smooth sliding, and since this cannot occur, we should have $\omega \geqslant 1$. On the other hand, it is very unlikely that $L_{\max}$ scales as a power of L_z larger than 1, because in a geometry of a slab of thickness L_z, a static perturbation at some point does not have an effect beyond some distance of the order of L_z. This takes us to the heuristic finding that the exponent effectively found in the numerical simulations, namely, $\omega = 1$, is the most natural result to be expected.

A further question that we asked ourselves concerning this point is the following. The OFC* model displays a behavior with $\omega = 1/2$, whereas our results for the OFCR model indicate $\omega = 1$. How is the transition between these two exponents as the precise value of R is varied between 0 (OFC*) and a large value (OFCR)? Although this is an attractive question to explore, some investigation of the possibilities to provide an answer based on numerical simulations convinced us that we are not able to do so at present. We want to stress, however, our expectation that an answer to this question could give insight into the puzzling problem of creeping faults [19], namely, a piece of a fault in which there is an almost-complete absence of earthquakes and the sliding is smooth, while earthquakes occur in adjacent segments of the same fault. In our view this could be related to an abrupt transition between $\omega = 1$ for a "normal" segment to a value of $\omega < 1$ in a creeping fault, and this abrupt transition could be driven by a smooth change in the amount of relaxation in the system. Clearly this issue is an open line for future research.

VI. WHY $b \simeq 1$?

One of the results that surprised us most concerning the OFCR model is the fact that it displays a realistic exponent $b \simeq 1$ ($\tau \simeq 1.67$), whereas the OFC* model has $b \simeq 0.4$ ($\tau \simeq 1.27$). This is surprising because the inclusion of relaxation was aimed at generating aftershocks (which it does), and not at obtaining a "correct" GR law. So we believe that it is necessary to provide an explanation for this behavior.

In Sec. III C we recovered Eq. (7) linking the avalanche exponent τ with the roughness exponent ζ of the events in the OFC* model. The steps followed there can be done also in the case of the OFCR model. The only important difference is that, as explained in the previous section, the scaling of $L_{\max} \sim (\alpha_c - \alpha)^{-\omega}$ has a different exponent for the OFCR case ($\omega = 1$) compared to the OFC* case ($\omega = 1/2$). The result that is obtained for a generic value of ω is

$$\tau = 2 - \frac{1/\omega}{2 + \zeta}. \tag{8}$$

This modified scaling relation suggests already a larger τ exponent in the OFCR case. In fact, assuming only a non-negative value for ζ, we get $\tau > 1.5$. To determine the value of ζ we need to characterize the internal structure of an avalanche. Four quantities can be used to this scope: (i) the already mentioned size S, which counts the total number of discharges; (ii) the area A, defined as the total number of blocks involved in the avalanche; (iii) the "duration" T, defined as the number of discharge steps that are necessary to exhaust the avalanche (note that sites that are critical at the same moment are discharged in parallel, in a single step); and (iv) the linear size L of the avalanche. Similarly to the size S, all these quantities are power law distributed up to a cutoff which depends on $\alpha_c - \alpha$. In the stationary regime, the study of the cutoff divergence, as the threshold α_c is approached, allows us to determine the value of the critical exponents like ζ, ν, ... A different approach, which does not rely on the stationary regime, consists in studying the behavior of A, T, and L as a function of the size S. For large S we expect a power-law behavior with $\langle A(S) \rangle \sim S^{\kappa_A}$, $\langle T(S) \rangle \sim S^{\kappa_T}$, and $\langle L(S) \rangle \sim S^{\kappa_L}$, where $\langle A(S) \rangle$ is the area averaged over all avalanches of size S, $\langle T(S) \rangle$ is the duration averaged over all avalanches of size S, and $\langle L(S) \rangle$ is the linear size averaged over all avalanches of size S. For the OFC* model, scaling relations predict, in two dimensions, $\kappa_A = \frac{2}{2+\zeta} \sim 0.73$, $\kappa_T = \frac{z}{2+\zeta} \sim 0.57$, and $\kappa_L = \frac{1}{2+\zeta} \sim 0.36$, where we have used the value $z = 1.56$ for the dynamical exponent. Numerical simulations in the OFC* model agree with these predictions. More surprisingly, also the avalanches in the OFCR model seem to have the same internal structure and the same value of the κ exponents. As the first consequence, if the value of ζ does not change appreciably from the value $\zeta \simeq 0.75$ in the absence of relaxation, through Eq. (8), we predict $\tau \simeq 1.64$, which is consistent with the value observed in the simulations (Fig. 6). On the other hand, the invariance of ζ when including relaxation gives a clue to the possible mechanism for the change of the τ exponent. In fact, if the new value of τ corresponds to the system being controlled by a different fixed point in the parameter space (i.e., a new universality class), we should expect that all exponents of the OFCR model are different from those in the OFC* model. However, as explained by Durin and Zapperi [20] in the context of a magnetic problem, if the internal (κ) exponents of the avalanches do not change, it is likely that the new τ exponent originates as an effect of nonstationarity. If there is in the model a parameter that samples a wide distribution of values, the complete event size distribution can be generated as an integration of partial distributions restricted to particular values of the parameter. If, for instance, this parameter controls the position of the cutoff of the distribution, such an integration produces a larger effective τ exponent but does not affect the exponents κ_A, κ_T, and κ_L characterizing the internal structure of the avalanches.

A parameter that widely fluctuates in the OFCR model is the stress σ. Since σ controls the position of the cutoff of the distribution in the OFC* model (see Fig. 5), an integration over all σ values could be the responsible of an overall power law with a larger decay exponent in the OFCR model. If this explanation is correct, the event size distribution restricted to some small stress interval should display a $\tau \simeq 1.27$, with a cutoff that is stress dependent. However, this is not the case. In Fig. 7(b) we show event size distributions restricted to the events in some of the individual clusters shown in Fig. 6 (and thus characterized by a single value of σ at triggering). We see for each individual cluster an event size distribution with the modified exponent $\tau \simeq 1.67$, indicating that σ is not the parameter over which the effective integration takes place. Some other, less obvious scheme of "integration over a parameter" may be responsible for the change in exponent.

We have not been able to identify clearly in the OFCR model the parameter that produces the effective integration. However, we have advanced toward this goal by doing the following simplified analysis. Let us consider a distribution of values of u and u^{th}. The thresholds are assumed to have an exponential distribution. The typical distribution of u and u^{th} in the absence of relaxation is sketched in Fig. 9(a). Note that instead of showing the actual values of uth, we show the distribution from which they are chosen. In the presence of relaxation, the values of the forces move as indicated in Fig. 9(b). In this process, any site for which $u_i < \sigma$ increases in value. As long as the actual value of uth is not reached, the probability distribution of uth continues to be exponential above u_i. If u_i reaches u_i^{th}, an aftershock is triggered. On the other hand, if $u_i > \sigma$ relaxation decreases the u_i value.
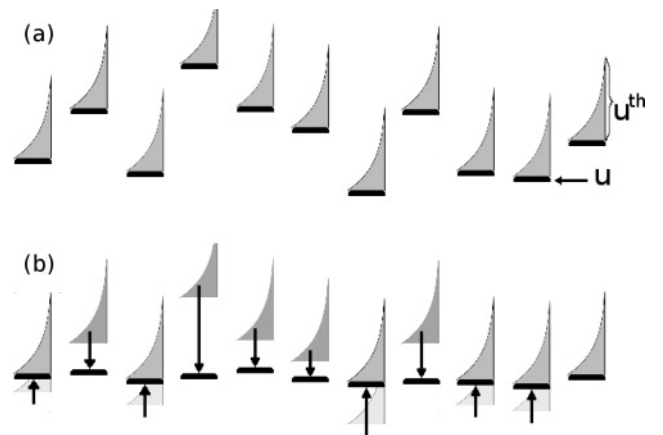

FIG. 9. (a) A typical distribution of forces u and thresholds u^{th} in the absence of relaxation. For u^{th} we show in gray the distribution from which each value is chosen, and not the values themselves. In the presence of relaxation, the configuration is modified as indicated in (b): sites for which relaxation produces an increase in u_i can trigger aftershocks. If not, the distribution of uth continues to be exponential. Sites for which relaxation produces a decrease in u_i get a gap between u and the lowest possible u^{th}, and these sites have a lower probability of being destabilized upon receiving a load from neighbors.
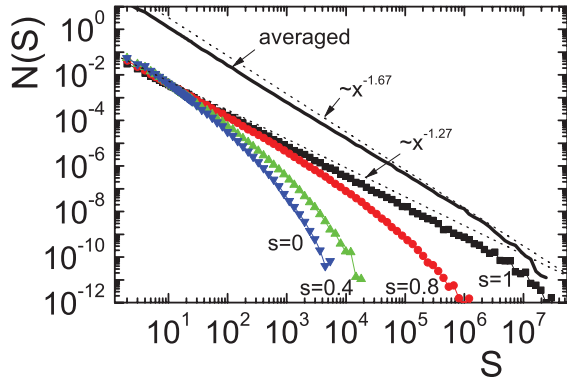
FIG. 10. (Color online) Avalanche size distribution for an uncorrelated distribution of u's and a shrink parameter s, as indicated. The distribution of u's is flat between $\bar{u} \pm \delta u$, with $\bar{u} = 1.29$ and $\delta u = 1$. The result of an integration over the parameter $0 < s < 1$ is shown by the line labeled "averaged" (vertically shifted, for convenience). As a reference, power laws with exponents 1.27 and 1.67 are also plotted.

To understand the effect of relaxation, and having in mind the previous scheme, we do the following simulation. We take uncorrelated values of u, from some distribution of width δu and mean $\bar{u}$, and take thresholds from an exponential distribution above the corresponding u, to mimic the configuration in Fig. 9(a). Then the values of u are shrunk toward σ by a factor s ($0 < s < 1$) to simulate the effect of relaxation, namely, $u \rightarrow \sigma + s(u - \sigma)$. If, in this process, u becomes larger than the corresponding u^{th}, the threshold is chosen again. In this final configuration we destabilize a site at random and measure the size of the avalanche that is generated. Statistics is collected on many realizations of the process. Results are shown in Fig. 10. For $s = 1$ (i.e., no relaxation) we get a power-law distribution with an exponent close to (actually, a bit larger than) the normal value $\tau \simeq 1.27$. As s is taken lower than 1, the distribution becomes steeper. The qualitative reason for this lies in the gaps that appear between the u values and the corresponding thresholds [Fig. 9(b)]: sites with larger gaps become less probable of being activated upon receiving a load from a neighbor.

By choosing s from a flat distribution between 0 and 1 (i.e., doing an integration over the value of s), a power-law decay is recovered, with an exponent similar to that found with the full OFCR model. In a full simulation with the OFCR model, one can imagine a situation in which each event occurs at a particular value of s, and an effective integration over this parameter occurs, generating the modified exponent. A full justification of this scenario is not trivial, and we expect to provide it elsewhere. In any case, our conclusion is that an effective integration over an internal parameter that is related to

relaxation may be responsible for the change of the τ exponent in the OFCR model.

VII. SUMMARY AND CONCLUSIONS

In this paper we have elaborated on the properties of a seismicity model that is based on the one proposed by OFC and that incorporates relaxation effects as a fundamental ingredient. In the past, this model was shown to generate realistic sequences of events, in particular, displaying aftershocks following an Omori law. It also generates a GR event size distribution with realistic power-law behavior and reproduces frictional properties experimentally observed in geological materials.

Here we have focused on the following issues. First, we have shown that there is a natural notion of a "seismic cycle" in the model. This occurs because the stress in the system has temporal variations that reflect the overall state of the plates, and we have found that mayor earthquakes can be expected only when this stress is larger than some minimum value. Second, we have made an analysis of the scaling of the largest events in the system upon system size increase. With appropriate interpretation of the parameter α of the model, it was suggested that, in fact, the size of the largest events scales as the system size (in particular, with the thickness of the plate we are trying to model). This indicates that the model is able to describe earthquakes in the macroscopic limit. Note that this is not true in the absence of relaxation, since in this case the largest events scale with system size with a power of <1.

Finally, we have tried to understand why relaxation is able to tune the exponent of the GR law to a realistic value around $b = 1$ (or $\tau \simeq 1.67$). We have provided evidence that the reason for this modification is mainly the creation of "gaps" between the u values and the corresponding thresholds u^{th}, originated in the existence of relaxation. Despite this qualitative understanding of the effect of relaxation, we have not been able to explain why the exponent of the GR law in the presence of relaxation seems to adjust systematically around the value $b \simeq 1$ (or $\tau \simeq 1.67$). Taken as a whole, the results presented in this paper reinforce our view that the relaxation mechanism introduced in some seismicity models provides an important tool for the study of seismic phenomena.

[1] R. Burridge and L. Knopoff, Bull. Seismol. Soc. Am. **57**, 341 (1967).

[2] J. M. Carlson, J. S. Langer, and B. E. Shaw, Rev. Mod. Phys. **66**, 657 (1994).

[3] Z. Olami, H. J. S. Feder, and K. Christensen, Phys. Rev. Lett. **68**, 1244 (1992).

[4] The OFC model does display aftershocks, but they are of a different nature than those observed experimentally, see the discussion in Ref. [6].

[5] E. A. Jagla, Phys. Rev. E **81**, 046117 (2010).

[6] E. A. Jagla and A. B. Kolton, J. Geophys. Res. **115**, B05312 (2010).

[7] T. Utsu, Y. Ogata, and R. S. Matsu'ura, J. Phys. Earth **43**, 1 (1995).

[8] C. Marone, Nature **391**, 69 (1998); Annu. Rev. Earth Planet. Sci. **26**, 643 (1998).

[9] H. Scholz, *The Mechanics of Earthquakes and Faulting* (Cambridge University Press, Cambridge, 2002).

[10] D. Cule and T. Hwa, Phys. Rev. Lett. **77**, 278 (1996).

[11] O. Narayan and A. A. Middleton, Phys. Rev. B **49**, 244 (1994).

[12] M. Paczuski and S. Boettcher, Phys. Rev. Lett. **77**, 111 (1996).

[13] T. Nattermann, S. Stepanow, L.-H. Tang, and H. Leschhorn, J. Phys. II **2**, 1483 (1992).

[14] O. Narayan and D. S. Fisher, Phys. Rev. B **48**, 7030 (1993).

[15] P. Le Doussal, K. J. Wiese, and P. Chauve, Phys. Rev. B **66**, 174201 (2002).

[16] A. B. Kolton, A. Rosso, T. Giamarchi, and W. Krauth, Phys. Rev. B **79**, 184207 (2009).

[17] O. Narayan, Phys. Rev. Lett. **77**, 3855 (1996).

[18] J. C. Ruegg, A. Rudloff, C. Vigny, R. Madariaga, J. B. de Chabalier, J. Campos, E. Kausel, S. Barrientos, and D. Dimitrov, Phys. Earth Planet. Inter. **175**, 78 (2009).

[19] F. Amelung and G. King, Geophys. Res. Lett. **24**, 507 (1997).

[20] G. Durin and S. Zapperi, J. Stat. Mech. (2006) P01002.